Coupled Systems Mechanics, *Vol. 10, No. 4 (2021) 317-331*
https://doi.org/10.12989/csm.2021.10.4.317

Delamination analysis of multilayered beams exhibiting creep under torsion

Victor I. Rizov*

Department of Technical Mechanics, University of Architecture, Civil Engineering and Geodesy, 1 Chr. Smirnensky blvd., 1046-Sofia, Bulgaria

(Received July 21, 2020, Revised June 15, 2021, Accepted June 23, 2021)

Abstract. A delamination analysis of a multilayered inhomogeneous beam structure under linear creep is developed. A viscoelastic model that consists of an arbitrary number of linear springs and linear dashpots is used. The cross-section of the beam is a circle. The beam is made of concentric longitudinal layers. Each layer is continuously inhomogeneous in thickness and length directions. Therefore, the shear moduli and the coefficients of viscosity of the viscoelastic model are distributed continuously along the thickness and length of each layer. Two concentric delamination cracks are located arbitrary between layers. The beam is loaded in torsion. Time-dependent solutions to the strain energy release rate for the two delaminations are derived by using the time-dependent strain energy in the beam. The strain energy release rates are derived also by the compliance method for verification. The variation of the strain energy release rate with time due to creep is evaluated. The effects of material inhomogeneity, external loading and delamination length on the strain energy release rate are investigated.

Keywords: creep; delamination; inhomogeneous material; multilayered beam; torsion

1. Introduction

The continuously inhomogeneous structural materials have drawn the attention of both practicing engineers and researchers during the last decades. These materials exhibit continuous (smooth) change of their properties along one or more directions in the solid (Tokovyy and Ma 2017, Tokovyy and Ma 2019, Tokovyy 2019). Therefore, the material properties are smooth functions of the coordinates. It should be noted that the strong interest to continuously inhomogeneous structural materials is conditioned by the wide entering of functionally graded materials in various areas of up-to-date engineering. Functionally graded materials represent a new kind of continuously inhomogeneous composites made by continuously mixing of two or more constituent materials (Akbaş 2017, 2018, 2019, Gasik 2010, Hedia *et al.* 2014, Hirai and Chen 1999, Mahamood and Akinlabi 2017, Miyamoto *et al.* 1999, Nemat-Allal *et al.* 2011, Uslu Uysal and Kremzer 2015, Uslu Uysal 2016, Uslu Uysal and Güven 2015, Vishesh Kar *et al.* 2016). One of the basic advantages of functionally graded materials in comparison with the conventional homogeneous structural materials is the fact that the former permit controlled tailoring of their microstructure and composition during the manufacturing with aim of obtaining of maximum

*Corresponding author, Professor, E-mail: V_RIZOV_FHE@UACG.BG

http://www.techno-press.org/?journal=csm&subpage=8 ISSN: 2234-2184 (Print), 2234-2192 (Online)

benefits from their continuous inhomogeneity. That is why the functionally graded materials are frequently used in critical structural applications in aeronautics, nuclear reactors, automotive industry and power plants.

The structural integrity and safety of continuously inhomogeneous (functionally graded) materials depend in a high degree on their fracture behavior (Dolgov 2005, 2016, Uslu Uysal and Güven 2016). Therefore, analyzing of various crack problems in continuously inhomogeneous structural members and components can aid significantly in the design and use of these novel composite materials especially in load-bearing structural applications. One of the specific disadvantages of multilayered inhomogeneous structures is the high risk of delamination fracture. Delamination crack problems in various beam configurations loaded in bending have been analyzed in (Hutchinson and Suo 1992). Solutions of the strain energy release rate have been derived assuming linear-elastic behavior of the materials. The beams considered in (Hutchinson and Suo 1992) have rectangular cross-section. However, multilayered beam structures of circular cross-section under torsion are also used in various load-bearing applications. Besides, these structures very often are subjected to constant external loadings for a long time. In such cases, the structures usually exhibit creep behavior. Therefore, delamination analyses of multilayered inhomogeneous beams of circular cross-section exhibiting creep under torsion have to be developed too.

The purpose of the present paper is to analyze the strain energy release rate for two concentric delamination cracks in a multilayered inhomogeneous beam of circular cross-section that exhibits linear creep behavior (the paper is motivated by the fact that previous analyses do not consider the effect of creep (Rizov 2017, 2018a, b, 2019a, b, 2020, Rizov and Altenbach 2020)). The beam is under torsion. The creep is treated by using a viscoelastic constitutive model consisting of an arbitrary number of linear springs and dashpots. The strain energy release rate is derived by using the time-dependent strain energy density. The strain energy release rate is obtained also by applying the compliance method. The results yielded by the two solutions are identical. The main benefit of the present work is that solutions of the strain energy release rate which account for the creep in a multilayered inhomogeneous beam with two delaminations under torsion are derived. The solutions are suitable for parametric studies. Also, the solutions can be applied to check for crack growth. The change of the strain energy release rate with the time due to the creep behavior is examined by using the solutions. The influence of material inhomogeneity, delamination lengths and the number of springs and dashpots in the model on the strain energy release rate is studied.

2. Strain energy release rate in viscoelastic multilayered inhomogeneous beam subjected to torsion

The beam shown in Fig. 1 is under consideration. The cross-section of the beam is a circle of radius, R_3. The beam is clamped in its right-hand end. The length of the beam is l. The beam is made of adhesively bonded concentric longitudinal layers which have different thicknesses and material properties. Two concentric delamination cracks are located arbitrary between layers as shown in Fig. 1. The lengths of the internal and external cracks are a_1 and a_2, respectively. The two cracks represent circular cylindrical surfaces of radiuses, R_1 and R_2. The crack fronts of the external and internal cracks are located in sections, H_2 and H_3, respectively. In portion, H_1H_2, the beam is divided by the two cracks in internal, interstitial and external parts. The internal part has a circular cross-section of radius, R_1. The interstitial and external parts of the beam have ring-shaped

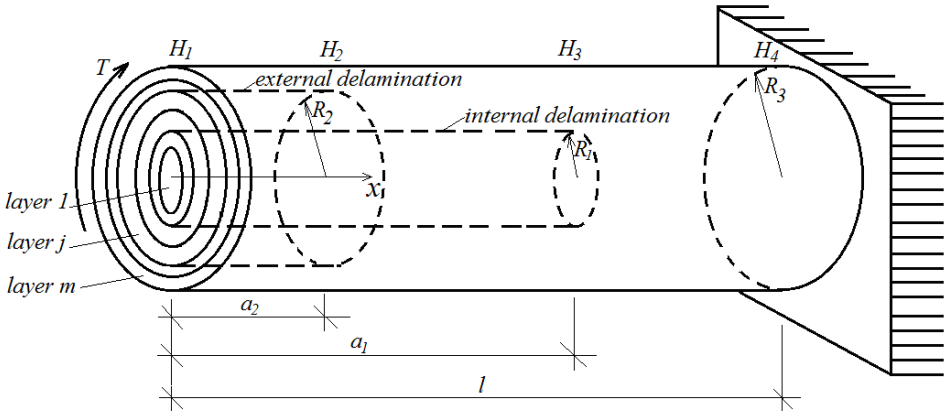

Fig. 1 Geometry and loading of a multilayered inhomogeneous cantilever beam with two circular cylindrical delaminations

cross-sections. The internal and external radiuses of the cross-section of the interstitial part are R_1 and R_2, respectively. The radiuses of the cross-section of the external part are R_2 and R_3, respectively. In portion, H_2H_3, the internal crack divides the beam in internal and external parts. The cross-section of the internal part is a circle of radius, R_1. The external part has a ring-shaped cross-section of internal and external radiuses, R_2 and R_3, respectively. The beam is loaded by a torsion moment, T, applied at the free end of the external part of the beam (Fig. 1). The internal and interstitial parts of the beam in portion, H_1H_2, and the internal part in portion, H_2H_3, are free of stresses.

The material in each layer of the beam exhibits linear creep behavior that is treated by using the generalized Kelvin viscoelastic model depicted in Fig. 2. The model consists of n linear dashpots and n+1 linear springs connected as shown in Fig. 2. Under constant applied shear stress, for the model in Fig. 2, the stress-strain-time relationship in the j-th layer of the beam is written as

$$\gamma = \frac{\tau_j}{G_j} + \tau_j \sum_{i=1}^{i=n} \frac{1 - e^{-\frac{t}{\lambda_{ji}}}}{G_{ji}}, \tag{1}$$

where

$$\lambda_{ji} = \frac{\eta_{ji}}{G_{ji}}, \tag{2}$$

$$j = 1, 2, \ldots m\,. \tag{3}$$

In the above formulae, γ is the shear strain, τ_j is the shear stress in the layer, G_{ji} is the shear modulus of the i-th spring, η_{ji} is the coefficient of viscosity of the i-th dashpot, t is time, m is the number of layers.

Each layer of the beam is made of material that is continuously inhomogeneous in both thickness and length directions. Therefore, the shear moduli and the coefficients of viscosity vary continuously along the thickness and length of the layer.

The following exponential laws are applied to describe the variation of the shear moduli and

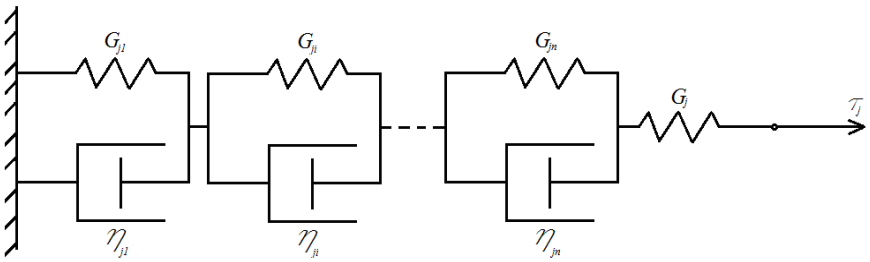

Fig. 2 Linear viscoelastic model

the coefficient of viscosity in the thickness direction of the *j*-th layer

$$G_j = G_{j0} e^{p_j \frac{R-R_{j-1}}{R_j-R_{j-1}}}, \tag{4}$$

$$G_{ji} = G_{ji0} e^{q_{ji} \frac{R-R_{j-1}}{R_j-R_{j-1}}}, \tag{5}$$

$$\eta_{ji} = \eta_{ji0} e^{g_{ji} \frac{R-R_{j-1}}{R_j-R_{j-1}}}, \tag{6}$$

where

$$R_{j-1} \le R \le R_j, \tag{7}$$

$$j = 1, 2, ...m, \tag{8}$$

$$i = 1, 2, ...n. \tag{9}$$

In formulae (4)-(7), G_{j0}, G_{ji0} and η_{ji0} are, respectively, the values of G_j, G_{ji} and η_{ji} at the internal surface of the layer, p_j, q_{ji} and g_{ji} are parameters which control the distribution of G_j, G_{ji} and η_{ji} in the thickness direction, R_{j-1} and R_j are the radiuses of the internal and external surfaces of the layer, respectively.

The distributions of G_{j0}, G_{ji0} and η_{ji0} along the length of the beam are written as

$$G_{j0} = G_{j0F} e^{f_j \frac{x}{l}}, \tag{10}$$

$$G_{ji0} = G_{ji0F} e^{b_{ji} \frac{x}{l}}, \tag{11}$$

$$\eta_{ji0} = \eta_{ji0F} e^{h_{ji} \frac{x}{l}}, \tag{12}$$

where

$$0 \le x \le l, \tag{13}$$

$$j = 1, 2, ...m, \tag{14}$$

$$i = 1, 2, ...n. \tag{15}$$

In formulae (10)-(12), G_{j0F}, G_{ji0F} and η_{ji0F} are, respectively, the values of G_{j0}, G_{ji0} and η_{ji0} at the

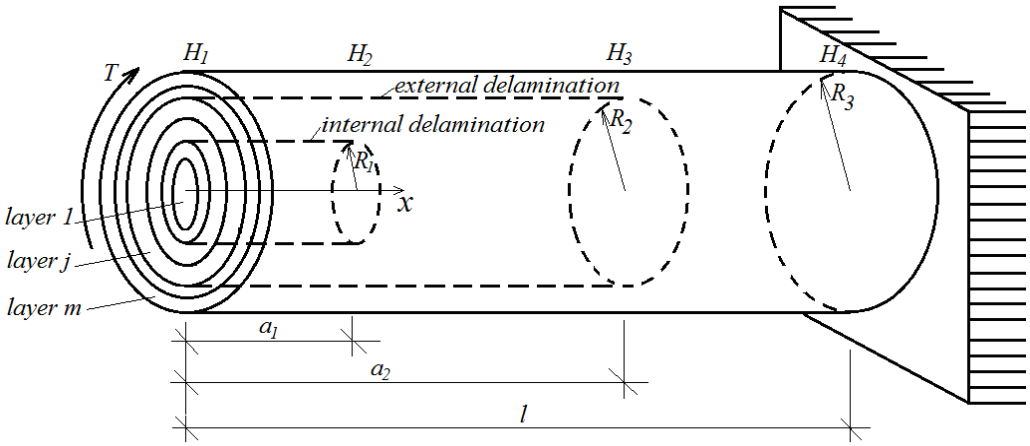

Fig. 3 Multilayered inhomogeneous cantilever in which the external delamination is longer than the internal one

free end of the beam, f_j, b_{ji} and h_{ji} are parameters which control the distribution of G_{j0}, G_{ji0} and η_{ji0} in the length direction, x is the longitudinal centroidal axis of the beam (Fig. 1).

The delamination is analyzed in terms of the strain energy release rate. For this purpose, first, a time-dependent solution to the strain energy release rate, G_{a_1}, is derived assuming an elementary increase, da_1, of the internal crack. The strain energy release rate is written as

$$G_{a_1} = \frac{dU}{2\pi R_1 da_1}, \tag{16}$$

where U is the time-dependent strain energy in the beam. Since the internal and interstitial parts of the beam in portion, H_1H_2, and the internal part in portion, H_2H_3, are free of stresses, the time-dependent strain energy is expressed as

$$U = U_1 + U_2 + U_3, \tag{17}$$

where U_1, U_2 and U_3 are, respectively, the strain energies cumulated in the external parts of portions, H_1H_2 and H_2H_3, of the beam and in the un-cracked beam potion, H_3H_4.

The strain energy in the external part of beam portion, H_1H_2, is obtained as

$$U_1 = \sum_{j=1}^{j=m_1} \int_0^{a_2} \int_{R_{j-1}}^{R_j} u_{01j} 2\pi R dR dx, \tag{18}$$

where m_1 is the number of layers in external part of the beam portion, H_1H_2, u_{o1_j} is the time-dependent strain energy density in the j-th layer. The following formula is used to calculate u_{o1_j}

$$u_{01j} = \frac{1}{2}\tau_j \gamma. \tag{19}$$

The distribution of the shear strain is treated by applying the Bernoulli's hypothesis for plane sections sine beams of high length to diameter ratio are considered in the present paper. Thus, the

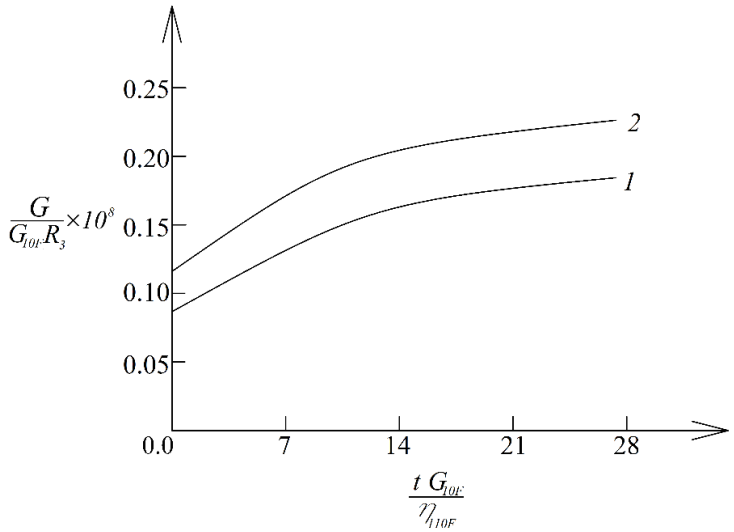

Fig. 4 The strain energy release rate in non-dimensional form plotted against the non-dimensional time (curve 1-for the internal delamination, curve 2-for the external delaminsation)

distribution of γ in radial direction of the external part of portion, H_1H_2, of the beam is written as

$$\gamma = \frac{\gamma_E}{R_3} R\,, \tag{20}$$

where

$$R_2 \le R \le R_3\,. \tag{21}$$

In formula (20), γ_E is the shear strain at the surface of the beam. The following equation for equilibrium of the elementary forces in the cross-section of the external part of beam portion, H_1H_2, is used to determine γ_E

$$T = \sum_{j=1}^{j=m_1} \int_{R_{j-1}}^{R_j} \tau_j 2\pi R^2 dR\,. \tag{22}$$

From (1), it follows that

$$\tau_j = \frac{\gamma}{\frac{1}{G_j} + \sum_{i=1}^{i=n} \frac{1-e^{-\frac{t}{\lambda_{ji}}}}{G_{ji}}} \tag{23}$$

By combining of (20) and (23), one derives

$$\tau_j = \frac{\gamma_E R}{R_3\left(\frac{1}{G_j} + \sum_{i=1}^{i=n} \frac{1-e^{-\frac{t}{\lambda_{ji}}}}{G_{ji}}\right)}, \tag{24}$$

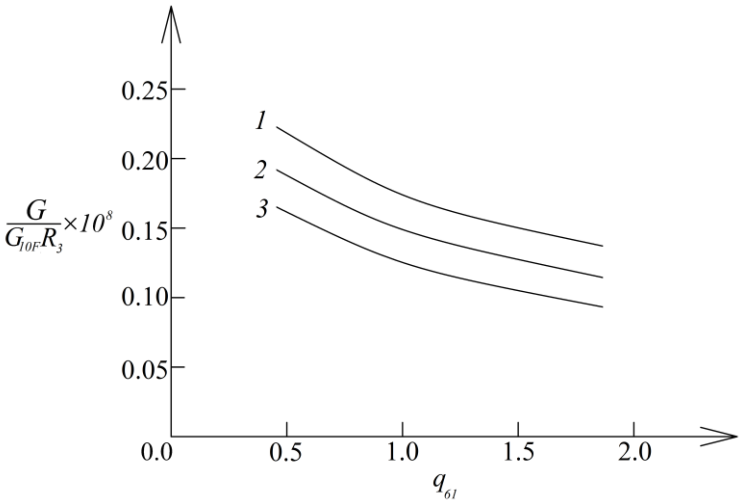

Fig. 5 The strain energy release rate in non-dimensional form plotted against q_{61} (curve 1-at g_{61}=0.5, curve 2-at g_{61}=0.7 and curve 3-at g_{61}=0.9)

where

$$R_{j-1} \le R \le R_j \,. \tag{25}$$

After substituting of (24) in (22), the equation for equilibrium is solved with respect to γ_E at various values of time by using the MatLab.

The time-dependent strain energy cumulated in the external part of portion, H_2H_3, of the beam is written as

$$U_2 = \sum_{j=1}^{j=m_2} \int_{a_2}^{a_1} \int_{R_{j-1}}^{R_j} u_{02j} 2\pi R dR dx \,, \tag{26}$$

where m_2 is the number of layers in the external part of beam portion, H_2H_3, u_{02j} is the time-dependent strain energy density that is obtained by replacing of γ with γ_I in formula (19). The distribution of γ_I is found by replacing of γ_E with γ_{EI} in (20). The shear strain, γ_{EI}, at the surface of the beam in portion, H_2H_3, is found by equation (22). For this purpose, m_1 and τ_j are replaced, respectively, with m_2 and τ_{jI} where τ_{jI} is the shear stress. The shear strain, γ_E, is replaced with γ_{EI} in (24) to find τ_{jI}.

The time-dependent strain energy in the un-cracked beam portion is found as

$$U_3 = \sum_{j=1}^{j=m} \int_{a_1}^{l} \int_{R_{j-1}}^{R_j} u_{03j} 2\pi R dR dx \,, \tag{27}$$

where the strain energy density, u_{03j}, is obtained by replacing of γ with γ_{II} in (19). Formula (20) is used to obtain γ_{II} by replacing of γ_E with γ_{EII}. Eq. (22) is applied to determine the shear strain, γ_{EII}, at the surface of the beam in the un-cracked portion. For this purpose, m_1 and τ_j are replaced with m and τ_{jII}, respectively. The shear stress, τ_{jII}, is found by replacing of γ_E with γ_{EII} in (24).

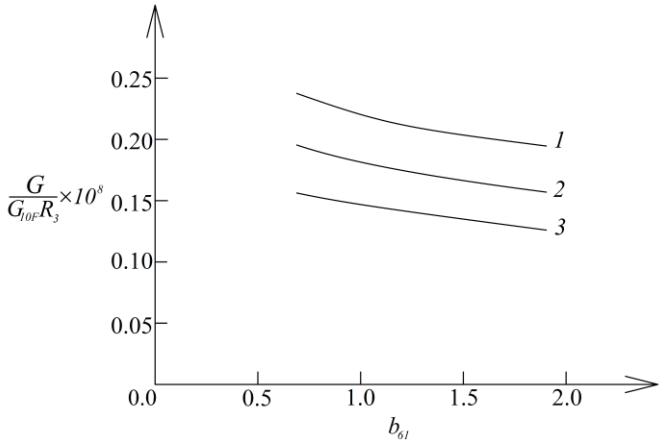

Fig. 6 The strain energy release rate in non-dimensional form plotted against b_{61} (curve 1-at h_{61}=0.4, curve 2-at h_{61}=0.6 and curve 3-at h_{61}=0.8)

By substituting of (18), (26) and (27) in (17) and then in (16), one obtains the following time-dependent solution to the strain energy release rate

$$G_{a_1}=\frac{1}{R_1}\left(\sum_{j=1}^{j=m_2}\int_{R_{j-1}}^{R_j}u_{02j}RdRdx-\sum_{j=1}^{j=m}\int_{R_{j-1}}^{R_j}u_{03j}RdRdx\right), \tag{28}$$

where the strain energy densities are found at $x=a_1$. The integration in (28) is carried-out by using the MatLab computer program. Solution (28) is applied to calculate the strain energy release rate at various values of time. In this way, the variation of the strain energy release rate with time due to the creep can be evaluated.

The strain energy release rate is derived also by applying the compliance method. According to this method, the strain energy release rate can be written as

$$G_{a_1}=\frac{1}{2}\frac{T^2}{l_{crf1}}\frac{dC}{da_1}, \tag{29}$$

where l_{crf1} is the front length of the internal crack, C is the compliance. The front length of the internal crack is found as

$$l_{crf1}=2\pi R_1. \tag{30}$$

By substituting of (30) in (29), one obtains

$$G_{a_1}=\frac{T^2}{4\pi R_1}\frac{dC}{da_1}. \tag{31}$$

The compliance is expressed as

$$C=\frac{\varphi}{T}, \tag{32}$$

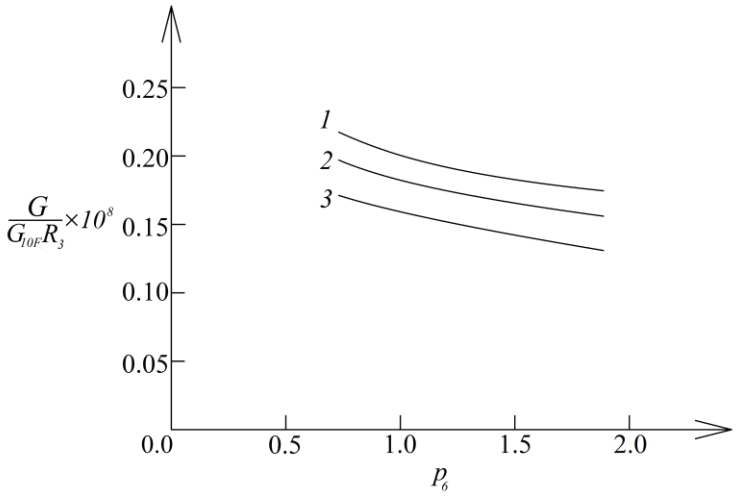

Fig. 7 The strain energy release rate in non-dimensional form plotted against p_6 (curve 1-at a_2/l=0.3, curve 2-at a_2/l=0.5 and curve 3-at a_2/l=0.7)

where φ is the angle of twist of the free end of the external part of beam portion, H_1H_2. This angle is obtained by applying the integrals of Maxwell-Mohr. The result is

$$\varphi = \int_0^{a_2} \frac{\gamma_E}{R_3} dx + \int_{a_2}^{a_1} \frac{\gamma_{EI}}{R_3} dx + \int_{a_2}^{l} \frac{\gamma_{EII}}{R_3} dx . \tag{33}$$

By combining of (31), (32) and (33), one derives the following solution to the strain energy release rate

$$G_{a_1} = \frac{T}{4\pi R_1}\left(\frac{\gamma_{EI}}{R_3} - \frac{\gamma_{EII}}{R_3}\right), \tag{34}$$

where γ_{EI} and γ_{EII} are obtained at $x=a_1$. It should be mentioned that the strain energy release rate found by (34) is exact match of that calculated by applying (28). This fact proves the correctness of the analysis of the strain energy release rate.

A time-dependent solution to the strain energy release rate is found also at increase of the external crack. For this purpose, (16) is re-written as

$$G_{a_2} = \frac{dU}{2\pi R_2 da_2} . \tag{35}$$

By substituting of (18), (26) and (27) in (35), one derives

$$G_{a_2} = \frac{1}{R_2}\left(\sum_{j=1}^{j=m_1} \int_{R_{j-1}}^{R_j} u_{01j} R dR dx - \sum_{j=1}^{j=m_2} \int_{R_{j-1}}^{R_j} u_{02j} R dR dx \right), \tag{36}$$

where the strain energy densities are obtained at $x=a_2$. The MatLab computer program is applied to perform the integration in (36).

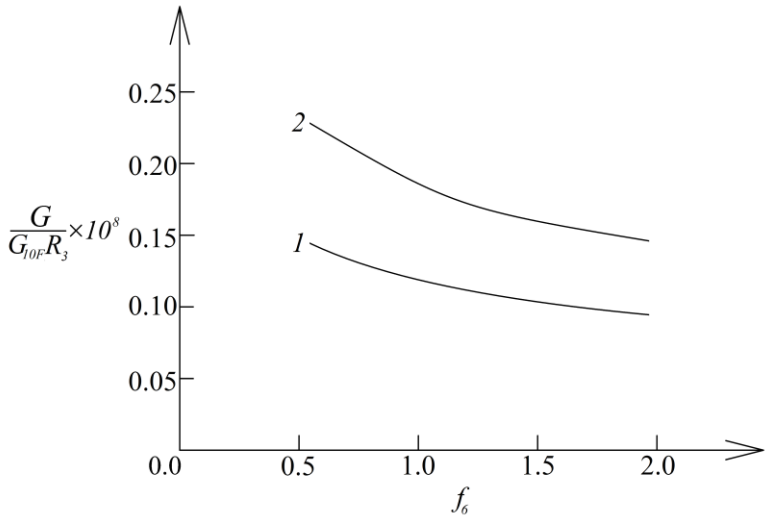

Fig. 8 The strain energy release rate in non-dimensional form plotted against f_6 (curve 1-at T=4 Nm, curve 2-at T=5 Nm)

The strain energy, G_{a_2}, is found also by using the compliance method. Expression (31) is re-written as

$$G_{a_2} = \frac{T^2}{4\pi R_2}\frac{dC}{da_2}. \tag{37}$$

By substituting of (32) and (33) in (37), one obtains

$$G_{a_2} = \frac{T}{4\pi R_2}\left(\frac{\gamma_E}{R_3} - \frac{\gamma_{EI}}{R_3}\right), \tag{38}$$

where γ_E and γ_{EI} are determined at $x=a_2$. The fact that the strain energy release rate calculated by using (38) is exact match of that found by (36) proves the correctness of the analysis of the strain energy release rate developed at increase of the external delamination crack.

The strain energy release rate is derived also for beam configuration in which the external delamination crack is longer than the internal one (Fig. 3). In this configuration, the fronts of the internal and external cracks are located in beam cross-sections, H_2 and H_3, respectively. It is obvious that the internal and interstitial parts of the beam in portion, H_1H_2, and the internal part of beam portion, H_2H_3, are free of stresses (Fig. 3). Therefore, the time-dependent strain energy cumulated in the beam is obtained as

$$U = \sum_{j=1}^{j=m_1}\int_0^{a_2}\int_{R_{j-1}}^{R_j} u_{01j}\,2\pi R dR dx + \sum_{j=1}^{j=m}\int_{a_2}^{l}\int_{R_{j-1}}^{R_j} u_{03j}\,2\pi R dR dx\,, \tag{39}$$

where the time-dependent strain energy density, u_{01j}, is found by applying formula (24). In order to calculate u_{03j}, γ_E is replaced with γ_{EII} in (24).

First, the strain energy release rate is derived assuming increase of the internal delamination

crack. For this purpose, (39) is substituted in (16). The result is G_{a_1}=0. This finding is attributed to the fact that the front of internal crack is located in zone that is free of stresses (internal and interstitial parts of beam portion, H_1H_2, and the internal part of the beam portion, H_2H_3, are free of stresses (Fig. 3)).

The strain energy release rate, G_{a_1}, is found also by using the compliance method. The angle of twist of the free end of external part of the beam that is needed to calculate the strain energy release rate by (31) is obtained by applying the integrals of Maxwell-Mohr

$$\varphi = \int_0^{a_2} \frac{\gamma_E}{R_3} dx + \int_{a_2}^{l} \frac{\gamma_{EII}}{R_3} dx . \tag{40}$$

By substituting of (40) in (31), one obtains G_{a_1}=0.

Formula (35) is applied to derive the strain energy release rate at increase of the external crack for the beam shown in Fig. 3. By combining of (35) and (39), one obtains

$$G_{a_2} = \frac{1}{R_2}\left(\sum_{j=1}^{j=m_1} \int_{R_{j-1}}^{R_j} u_{01j} R dR dx - \sum_{j=1}^{j=m} \int_{R_{j-1}}^{R_j} u_{03j} R dR dx \right), \tag{41}$$

where the strain energy densities are determined at $x=a_2$. The integration in (41) is performed by the MatLab computer program. Solution (41) can be used to calculate the strain energy release rate at various values of time.

The compliance method is also applied to obtain G_{a_2}. For this purpose, by substituting of (40) in (37), one derives

$$G_{a_2} = \frac{T}{4\pi R_2}\left(\frac{\gamma_E}{R_3} - \frac{\gamma_{EII}}{R_3} \right), \tag{42}$$

where γ_E and γ_{EII} are found at $x=a_2$. It should be mentioned that the strain energy release rate obtained by (42) is exact match of that determined by (41) which proves the correctness of the analysis.

3. Parametric study

A parametric study of the delamination is performed in this section of the paper. For this purpose, calculations of the strain energy release rate are carried-out by applying the time-dependent solutions to the strain energy release rate derived in the previous section. The strain energy release rate is expressed in non-dimensional form by using the formula $G_N=G/(G_{10F}R_3)$. The purpose of the parametric study is to evaluate the variation of the strain energy release rate with time due to the creep behavior of the multilayered inhomogeneous beam under torsion. The effects of material inhomogeneity, the lengths of the two delamination cracks and the external loading on the strain energy release rate are evaluated too. It is assumed that l=0.250 m, R_3=0.006 m, T=5 Nm, m_1=2, m_2=4, m=6, n=3 (i.e., the viscoelastic model used consists of 3 dashpots and 4 springs), p_j=0.6, q_{ji}=0.7, g_{ji}=0.8, f_j=0.5, b_{ji}=0.7 and h_{ji}=0.8 where j=1,2,…6, i=1,2,3. The thickness of each layer is 0.001 m.

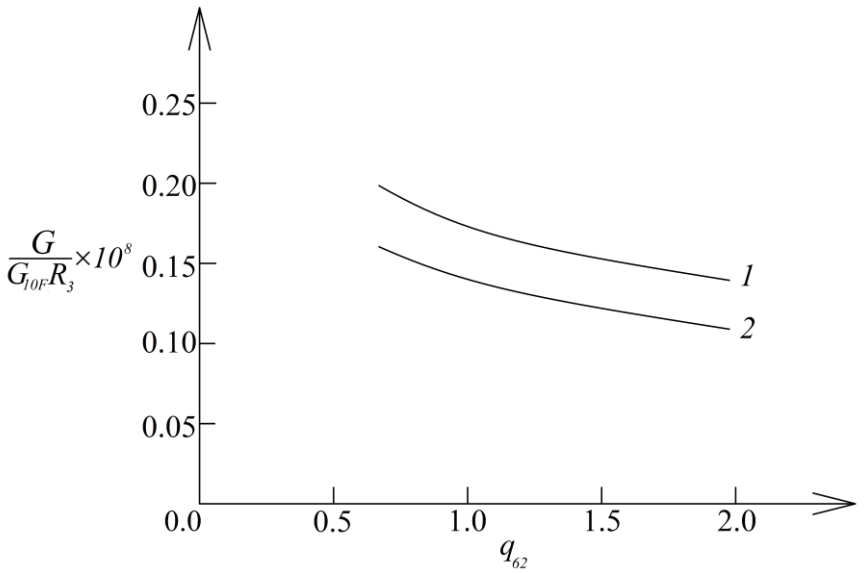

Fig. 9 The strain energy release rate in non-dimensional form plotted against q_{62} (curve 1- for the beam configuration with shorter external delamination (Fig. 1), curve 2 - for the beam configuration with longer external delamination (Fig. 2)

First, the variation of the strain energy release rate with time is investigated for the beam configuration in which the internal crack is longer than the external one (Fig. 1). For this purpose, calculations of the strain energy release rate are carried-out at various values of time by using solutions (28) and (36). The results obtained are illustrated in Fig. 4 where the strain energy release rate in non-dimensional form is plotted against the non-dimensional time. The time is presented in non-dimensional form by using the formula $t_N=tG_{10F}/\eta_{110F}$. One can observe in Fig. 4 that the strain energy release rate increases with time (this is due to the creep behavior). It can also be observed in Fig. 4 that the strain energy release rate for the external delamination crack is higher than that for the internal crack. It should be mentioned that the strain energy release rate at $t_N=0$ is due to the instantaneous linear-elastic strain that is modeled by the spring whit shear modulus G_j (Fig. 1).

The effect of the material inhomogeneity in the thickness direction is analyzed. For this purpose, calculations of the strain energy release rate are performed at various values of q_{61} and g_{61} by using the solution to the strain energy release rate derived at increase of the external crack in the beam configuration shown in Fig. 1. The strain energy release rate in non-dimensional form is plotted against q_{61} in Fig. 5 at three values of g_{61}. It is evident from Fig. 5 that the strain energy release rate decreases with increasing of q_{61}. One can observe in Fig. 5 that the increase of g_{61} leads also to decrease of the strain energy release rate.

The effect of the material inhomogeneity in the length direction is analyzed too. The solution to the strain energy release rate derived at increase of the external delamnation in the beam in Fig. 1 is used to carry-out calculations at various values of b_{61} and h_{61}. The calculated strain energy release rate is plotted in non-dimensional form against b_{61} in Fig. 6 at three values of h_{61}. The curves in Fig. 6 indicate that the strain energy release rate decreases with increasing of b_{61}. The increase of material property, h_{61}, leads also to decrease of the strain energy release rate (Fig. 6).

The influence of the delamination length is investigated. Calculations of the strain energy

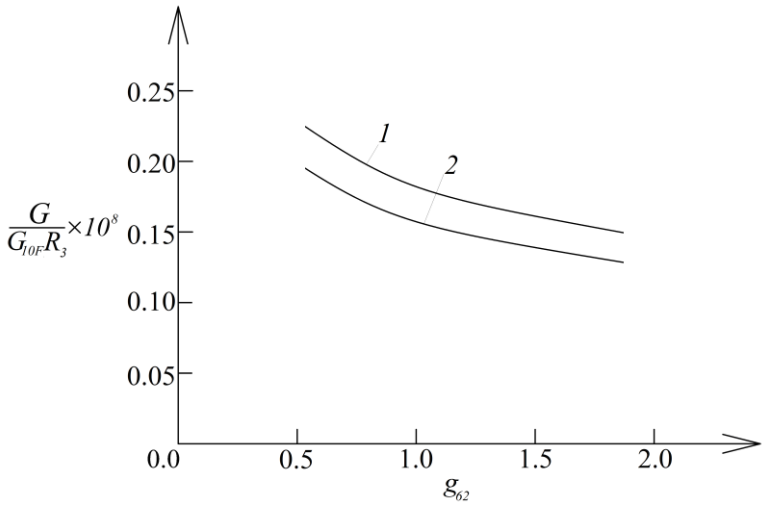

Fig. 10 The strain energy release rate in non-dimensional form plotted against g_{62} (curve 1-at n=3, curve 2-at n=4)

release rate are carried-out by applying the solution obtained at increase of the external delamination crack in the multilayered beam configuration shown in Fig. 1. The strain energy release rate in non-dimensional form is plotted against p_6 in Fig. 7 at three a_2/l ratios. The curves in Fig. 7 show that the strain energy release rate decreases with increasing of a_2/l ratio (this behavior is due to the increase of the values of shear moduli and the coefficients of viscosity in the beam cross-sections in which the front of the external delamination crack is located). It can also be observed in Fig. 7 that the strain energy release rate decreases with increasing of p_6.

The influence of the torsion moment is studied. The solution to the strain energy release rate obtained at increase of the external delamination crack in the beam in Fig. 1 is used to perform calculations at various values of the torsion moment and the material property, f_6. The strain energy release rate in non-dimensional form is plotted against f_6 in Fig. 8 at two values of the torsion moment. One can observe that the strain energy release rate increases with increasing of the torsion moment (Fig. 8). The curves in Fig. 8 indicate that the strain energy release rate decreases with increasing of f_6.

It is important to compare the strain energy release rates in the beam configurations shown in Fig. 1 and Fig. 3. For this purpose, the strain energy release rate calculated by using the solutions derived at increase of the external crack in the two beam configurations are plotted in non-dimensional form against q_{62} in Fig. 9.

One can observe in Fig. 9 that the strain energy release rate for the beam configuration with shorter external crack (Fig. 1) is higher than that for the beam with longer external crack (Fig. 3).

The strain energy release rate is analyzed also by using a viscoelastic model consisting of 5 springs and 4 dashpots (i.e., n=4). In order to evaluate the influence of the number of springs and dashpots in the model used, the strain energy release rate in non-dimensional form is plotted against g_{62} in Fig. 10 for both n=3 and n=4. It is evident from Fig. 10 that the strain energy release rate obtained by using the viscoelastic model with 5 springs and 4 dashpots is higher than that found by the model with 4 springs and 3 dashpots (this finding is attributed to increase of the strains).

4. Conclusions

Multilayered inhomogeneous cantilever beam of circular cross-section with two delaminations exhibiting linear creep behavior under a torsion moment is analyzed. Time-dependent solutions of the strain energy release rate which take into account the creep behavior are derived for both delaminations. The solutions are verified by the compliance method. The solutions are applied to analyze the strain energy release rate. It is found that the strain energy release rate increases with time as a result of creep. The analysis reveals that the strain energy release rate for the external delamination is higher than that for the internal delamination. The study indicates that the strain energy release rate decreases with increasing of q_{61}, g_{61}, q_{62}, p_6 and g_{62} (the material properties, q_{61}, g_{61}, q_{62}, p_6 and g_{62}, control the distributions of the coefficients of viscosity and the shear moduli along the thickness). It is found also that the increase of material properties, b_{61}, h_{61} and f_6, leads to decrease of the strain energy release rate. Concerning the effect of delamination length, the calculations show that the strain energy release rate decreases with increasing of a_2/l ratio. The analysis indicates that the strain energy release rate for the beam configuration with shorter external delamination is higher than that for the beam configuration with longer external delamination. The effect of the number of dashpots and springs in the linear creep model on the strain energy release rate is analyzed too. It is found that the strain energy release rate increases with increasing of the number of dashpots and springs in the model.

References

Akbaş, Ş.D. (2017), "Nonlinear static analysis of functionally graded porous beams under thermal effect", *Coupl. Syst. Mech.*, **6**(4), 399-415. https://doi.org/10.12989/csm.2017.6.4.399.

Akbaş, Ş.D. (2018), "Nonlinear thermal displacements of laminated composite beams", *Coupl. Syst. Mech.*, **7**(6), 691-705. https://doi.org/10.12989/csm.2018.7.6.691.

Akbaş, Ş.D. (2019), "Hygro-thermal post-buckling analysis of a functionally graded beam", *Coupl. Syst. Mech.*, **8**(5), 459-471. https://doi.org/10.12989/csm.2019.8.5.459 459.

Dolgov, N.A. (2005), "Determination of stresses in a two-layer coating", *Strength Mater.*, **37**(2), 422-431. https://doi.org/10.1007/s11223-005-0053-7.

Dolgov, N.A. (2016), "Analytical methods to determine the stress state in the substrate–coating system under mechanical loads", *Strength Mater.*, **48**(1), 658-667. https://doi.org/10.1007/s11223-016-9809-5.

Gasik, M.M. (2010), "Functionally graded materials: bulk processing techniques", *Int. J. Mater. Prod. Technol.*, **39**(1-2), 20-29. https://doi.org/10.1504/IJMPT.2010.034257.

Hedia, H.S., Aldousari, S.M., Abdellatif, A.K. and Fouda, N.A. (2014), "New design of cemented stem using functionally graded materials (FGM)", *Biomed. Mater. Eng.*, **24**(3), 1575-1588. https://doi.org/10.3233/BME-140962.

Hirai, T. and Chen, L. (1999), "Recent and prospective development of functionally graded materials in Japan", *Mater Sci. Forum*, **308-311**(4), 509-514. https://doi.org/10.4028/www.scientific.net/MSF.308-311.509.

Hutchinson, J. and Suo, Z. (1992), "Mixed mode cracking in layered materials", *Adv. Appl. Mech.*, **64**, 804-810.

Kar, V.R., Panda, S.K. and Mahapatra, T.R. (2016), "Thermal buckling behaviour of shear deformable functionally graded single/doubly curved shell panel with TD and TID properties", *Adv. Mater. Res.*, **54**, 205-221. https://doi.org/10.12989/amr.2016.5.4.205 205.

Mahamood, R.M. and Akinlabi, E.T. (2017), *Functionally Graded Materials*, Springer.

Miyamoto, Y., Kaysser, W.A., Rabin, B.H., Kawasaki, A. and Ford, R.G. (1999), *Functionally Graded*

Materials: Design, Processing and Applications, Kluwer Academic Publishers, Dordrecht/London/Boston.

Nemat-Allal, M.M., Ata, M.H., Bayoumi, M.R. and Khair-Eldeen, W. (2011), "Powder metallurgical fabrication and microstructural investigations of Aluminum/Steel functionally graded material", *Mater. Sci. Appl.*, **2**(5), 1708-1718. https://doi.org/10.4236/msa.2011.212228.

Rizov, V. and Altenbach, H. (2020), "Longitudinal fracture analysis of inhomogeneous beams with continuously varying sizes of the cross-section along the beam length", *Frattura ed Integrità Strutturale*, **53**, 38-50. https://doi.org/10.3221/IGF-ESIS.53.04.

Rizov, V.I. (2017), "Analysis of longitudinal cracked two-dimensional functionally graded beams exhibiting material non-linearity", *Frattura ed Integrità Strutturale*, **41**, 498-510. https://doi.org/10.3221/IGF-ESIS.41.61.

Rizov, V.I. (2018), "Analysis of cylindrical delamination cracks in multilayered functionally graded non-linear elastic circular shafts under combined loads", *Frattura ed Integrità Strutturale*, **46**, 158-17. https://doi.org/10.3221/IGF-ESIS.46.16.

Rizov, V.I. (2018), "Non-linear longitudinal fracture in a functionally graded beam", *Coupl. Syst. Mech.*, **7**(4), 441-453. https://doi.org/10.12989/csm.2018.7.4.441.

Rizov, V.I. (2019), "Influence of material inhomogeneity and non-linear mechanical behavior of the material on delamination in multilayered beams", *Frattura ed Integrità Strutturale*, **47**, 468-481. https://doi.org/10.3221/IGF-ESIS.47.37.

Rizov, V.I. (2019), "Influence of sine material gradients on delamination in multilayered beams", *Coupl. Syst. Mech.*, **8**(1), 1-17. https://doi.org/10.12989/csm.2019.8.1.001.

Rizov, V.I. (2020), "Delamination of multilayered non-linear elastic shafts in torsion", *FME Tran.*, **48**(3), 681-687. https://doi.org/10.5937/fme2003681R.

Tokovyy, Y. (2019), "Solutions of axisymmetric problems of elasticity and thermoelasticity for an inhomogeneous space and a half space", *J. Math. Sci.*, **240**(1), 86-97. https://doi.org/10.1007/s10958-019-04337-3.

Tokovyy, Y. and Ma, C.C. (2017), "Three-dimensional elastic analysis of transversely-isotropic composites", *J. Mech.*, **33**(6), 821-830. https://doi.org/10.1017/jmech.2017.91.

Tokovyy, Y. and Ma, C.C. (2019), "Elastic analysis of inhomogeneous solids: history and development in brief", *J. Mech.*, **18** (1), 1-14. https://doi.org/10.1017/jmech.2018.57.

Uslu Uysal, M. (2016), "Buckling behaviours of functionally graded polymeric thin-walled hemispherical shells", *Steel Compos. Struct.*, **21**(1), 849-862. https://doi.org/10.12989/scs.2016.21.4.849.

Uslu Uysal, M. and Güven, U. (2015), "Buckling of functional graded polymeric sandwich panel under different load cases", *Compos. Struct.*, **121**, 182-196. https://doi.org/10.1016/j.compstruct.2014.11.012.

Uslu Uysal, M. and Güven, U. (2016), "A bonded plate having orthotropic inclusion in adhesive layer under in-plane shear loading", *J. Adhes.*, **92**, 214-235. https://doi.org/10.1080/00218464.2015.1019064.

Uslu Uysal, M. and Kremzer, M. (2015), "Buckling behaviour of short cylindrical functionally gradient polymeric materials", *Acta Physica Polonica*, **A127**, 1355-1357. https://doi.org/10.12693/APhysPolA.127.1355.

AI